FISEVIER

Contents lists available at ScienceDirect

Additive Manufacturing

journal homepage: www.elsevier.com/locate/addma



Research Paper

Unsupervised learning for the droplet evolution prediction and process dynamics understanding in inkjet printing



Jida Huang^a, Luis Javier Segura^b, Tianjiao Wang^b, Guanglei Zhao^b, Hongyue Sun^{b,*}, Chi Zhou^{b,*}

- ^a Department of Mechanical and Industrial Engineering, University of Illinois at Chicago, Chicago, IL 60607, United States
- ^b Department of Industrial and Systems Engineering, University at Buffalo, SUNY Buffalo, NY 14260, United States

ARTICLE INFO

Keywords: Inkjet printing Unsupervised learning Deep recurrent neural network (DRNN) Video prediction Latent space decoding

ABSTRACT

Droplet jetting behavior largely determines the final drop deposition quality in the inkjet printing process. Forming such behavior is governed by the fluid flow pattern. Therefore, a measurement of the flow pattern is of great importance for improving the printing quality of the inkjet printing process. Most of the current works use static images for the study of the drop evolution process. The problem of the static images is that the images cannot recognize the motion information (i.e., temporal transformation) of the droplet. Thus the information of the jetting process in the temporal domain will be lost. Instead of using the images, this paper takes the video data as the study subject to investigate the droplet evolution behavior in the inkjet printing process. Moreover, this paper introduces a deep learning method for the study of such video data. Compared to most of the current learning approaches conducted in a supervised/semi-supervised manner for manufacturing process data, we propose an unsupervised learning method for studying the flow pattern of the droplet, which does not require well-defined ground-truth labels. Regarding the spatial and temporal transformation of the droplet in video data, we apply a deep recurrent neural network (DRNN) to implement the proposed unsupervised learning. To verify the hypothesis that the proposed method can learn a latent representation for reproducing original data, the proposed DRNN is trained and tested on both simulation and experimental datasets. Experimental results demonstrate that the proposed method can learn latent representations of the droplet jetting process video data, which is very useful for the prediction of the droplet behavior. Furthermore, through latent space decoding, the learned representations can infer the droplet forming stimulus parameters such as material properties, which would be very helpful for further understanding of the process dynamics and achieving real-time in-situ droplet deposition quality monitoring and control.

1. Introduction

Additive manufacturing (AM) is becoming one of the disruptive technologies for today's design and manufacturing industry. Among various AM technologies, inkjet printing has many attractive features such as non-contact, high resolution, low cost, and scalability to large area manufacturing [1]. Borrowing the concept from graphic arts and newspaper industry, inkjet printing allows for the deposition of versatile materials that enable its direct writing attribute. By virtue of such flexibility for multi-material and multi-functional capabilities, inkjet printing has been extensively deployed in broad applications within health, energy, environment, and electronics areas for the fabrication of multi-material and multi-functional products such as sensors, optic/ electronic devices and biochips [2–6].

Inkjet printing selectively ejects liquid-phase materials to the

substrate to form the final product. The process involves the ejection of a fixed quantity of liquid material in a chamber, from a nozzle through a sudden, quasi-adiabatic reduction of the chamber volume via piezo-electric action [1]. Responding to the external voltage, the liquid in the chamber is contracted, and the sudden reduction leads to a shockwave in the liquid, which causes a liquid drop ejecting from the nozzle [7]. The ejected drop falls under the action of gravity and air resistance until it reaches on the substrate [8]. An illustration of this process is shown in Fig. 1. Among various inkjet printing processes, the drop-on-demand (DOD) method can achieve the highest resolution reported so far [9]. A suitable technology to produce droplets in DOD mode is the piezo-electric inkjet (PIJ) process. In the PIJ process, the droplet formation is governed by tuning the driving electrical signal, various ink properties (e.g., surface tension, viscosity, density, etc.), and the interaction between the ink, air, and substrate (e.g., wettability of the nozzle)

E-mail addresses: hongyues@buffalo.edu (H. Sun), chizhou@buffalo.edu (C. Zhou).

^{*} Corresponding authors.

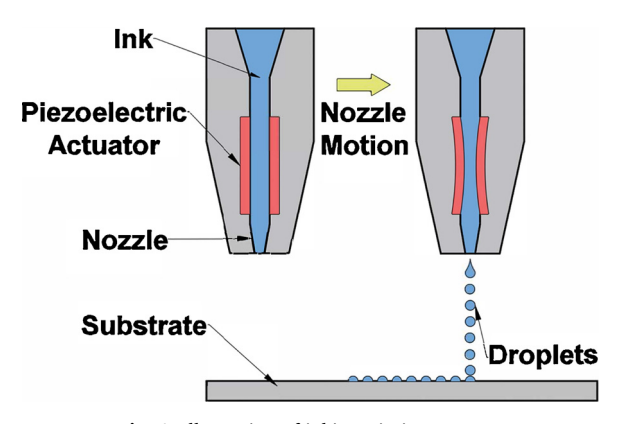


Fig. 1. Illustration of inkjet printing process.

[10,11]. Affected by many factors such as fluid properties, jetting conditions, and ambient properties, the PIJ process usually requires a careful-designed and subtle controlling system. Therefore, the most challenging part of inkjet printing is achieving a consistent droplet deposition quality, i.e., the reliability and repeatability of the jetting process, especially when the mass-production of inkjet-printed products is needed.

Many works have been attempted to investigate the governing mechanism of the droplet formation to address these challenges. These works mainly include two categories, physical-driven understanding, and sensing methods. Physical-based methods tend to find the fundamental flow of fluid ink and its properties. For example, several works used the computational fluid dynamics modeling on the measurements of material properties [12] (e.g., viscosity) and process parameters [13] (e.g., contact angle), other works studied the effect of pulse voltage on droplet behaviors [14]. While the sensing-based methods tried to improve the process quality and reliability through collecting and analyzing the in-situ process data. For instance, one feedback-feedforward control system was developed to stabilize the operating conditions of the electrohydrodynamic jet printing process in [15]. Heterogeneous sensors were used to achieve the online real-time quality monitoring for the AM process in [16]. However, when considering the droplet formation behavior of the jetting process, these approaches exhibited several shortcomings. First of all, physical-driven fluid modeling is inherently approximate and lack of direct measurements of fluid flow patterns, which is revealed critical for inkjet printing processes [1]. Furthermore, many other experimental based methods only consider a limited process or material parameters on the effect of droplet forming. It is challenging to get a comprehensive understanding of droplet jetting behavior and achieve optimal printing quality. Secondly, previous sensing-based methods usually do not offer direct handling of the actual flow pattern. Direct imaging provides a direct measurement of ink flow patterns. Hence, several works used the vision-based system for the study of flow pattern, e.g., a visualization system of drop-on-demand inkiet to observe the drop formation and deposition is developed in [17], and [18] proposed an in-process monitoring system for the electrohydrodynamic inkjet printing using machine vision. Imaging system was used to monitor the droplet formation process and study the pinchoff locations for inkjet printing [19], and predictive models were developed to predict droplet velocity and volume using ensemble learning [20]. These works use the static images as the study subjects, while the droplet forming process contains the motion of the drop and its temporal evolution, which could not be captured by the images. Therefore, to avoid this problem, this paper proposes to use the video as the study subject, i.e., the video of the droplet ejecting process in the PIJ process is captured for the measurement of the ink flow pattern. Compared to the static images used by most existing works [18,21,22], the video data of the printing process could reflect the motion of the flow pattern. In addition, the temporal information in the video data can significantly

contribute to the motion of the observed drop and its transformation undergoing [23,24].

Based on the collected vision data, the information embedded in the process can be extracted and then further utilized for the process monitoring and control. Usually, the size of the collected vision data is vast, especially for the video data. With such large data size, many works have been attempted to solve problems in the process monitoring and analysis of vision data by using machine learning methods, especially with impressive advancement of deep learning methods in recent years. For example, [25] presented the anomaly detection and classification method by using a trained computer vision algorithm. Similarly, the application of a supervised machine learning method for defect detection using high-resolution imaging was presented in [21]. Despite the superb performance of machine learning methods for vision data in AM process monitoring, most of the current works mainly exploit learning in a supervised manner. Supervised learning requires a large amount of labeled data, which is usually not easy to collect and define the ground-truth ones. Even the semi-supervised learning mode [26] still requires extensive labeled training data to improve network performance. To eliminate such tedious and laborious effort of defining ground-truth labels, representing the vision data in an unsupervised way can primarily facilitate the integration of deep learning methods with the video-based process monitoring in AM field.

The captured liquid droplet video data are used to investigate the flow pattern of the ink drop. For exploiting the unsupervised learning of the video data, the critical insight is that the underlying pattern of the video data, i.e., the morphology of the droplet and its evolution during the ejecting process, can be learned. Thus, in this paper, we hypothesize that with a deep recurrent neural network (DRNN), we can extract such a pattern of the drop, i.e., the droplet morphology and its phase transformations, from the recorded video data. To test this hypothesis, the learned representation is used to predict the future image frames of the observing object. Then the predicted frames are compared with the ones in the video itself. Accordingly, we can estimate the prediction error and evaluate the performance of the unsupervised learning method.

For the DRNN, a specialized network structure named PredNet [27], inspired by the predictive coding concept from neuroscience [28-30], is deployed for the unsupervised learning of the droplet jetting in PIJ process. To demonstrate that the proposed method can learn the flow pattern of the droplet in the jetting process, we firstly use a simulation method to generate synthetic videos from several predefined material parameters including density, viscosity, and surface tension. Then through the PredNet for synthetic data learning, the extracted latent representation is used to predict the future frames of the drop evolution. Experimental results show that the proposed method exhibits predicting capabilities for the ink flow pattern. This is important for achieving the consistent droplet deposition quality as the predicted flow behavior can be used for printing process stabilization, e.g., with in-situ process compensation and correction based on the predicted defects of the droplet. Consistent with the hypothesis, through decoding the latent generative model of the DRNN to investigate what the model has learned, we found that the proposed method can successfully learn the internal representations of flow patterns, which is very useful for the recognition of process governing parameters. This is also significant since if we can learn the underlying dynamics of the droplet flow pattern, the video-based unsupervised learning method can provide insightful guidance for designing the process and material parameters to achieve optimized printing quality. Lastly, the proposed method is extended to the study of the actual inkjet printing process video data. Experimental results verify the prediction effectiveness of the proposed method. It is demonstrated that the proposed method can successfully learn the latent representation of the droplet flow pattern in the inkjet printing process. Such latent representation is useful for estimating process parameters such as voltage and air pressure. To this end, the main contribution of this paper can be summarized as follows:

- The video data of the inkjet printing process is used as the study subject for investigating the flow pattern and droplet evolution. An unsupervised learning framework is proposed for the study of collected video data to extract the spatial and temporal information embedded in the data.
- The DRNN can learn the internal representation of the process video, such a representation in latent space is useful for the forecasting of droplet jetting behavior.
- 3. The proposed method can successfully predict droplet evolution behavior. Furthermore, the learned latent representations support estimating many hard-to-measure parameters (e.g., voltage and air pressure) in the printing process.

The remaining parts of this paper are organized as follows: Section 2 summarizes the related works on in-process monitoring of AM and machine learning-based methods. Section 3 presents the designed framework for PIJ process monitoring. The experimental results and discussion are demonstrated in Section 4. Finally, Section 5 concludes the paper.

2. Related work

2.1. In-situ process monitoring devices of additive manufacturing

The in-situ process monitoring for AM processes is under prompt development in recent years [31]. Various kinds of sensors and devices are instrumented in the AM processes for in-situ process monitoring [31–33]. For fused deposition modeling or fused filament fabrication process, an integrated measurement system including thermocouple, IR sensor, accelerometer, and camera were developed [16,34]. These sensors provided coupled information for process defects modeling and monitoring. For metal AM processes such as laser powder bed fusion (LPBF) and selective laser melting (SLM), thermal imaging [35], pyrometer [31], high-speed imaging [36], and acoustic sensing [37] were widely used. Novel sensing systems such as inline coherent imaging of depth [38], neutron diffraction measurement of residual strains and stresses [39], and laser ultrasonics measurement of material discontinuities and material thickness [31] were also proposed.

For the inkjet printing process, which is the focus of this paper, a machine vision system was designed to allow for printheads calibration, 3D scanning, and process control of a multi-material printing platform [40]. The droplet formation process of low, medium, and high viscosity inks were investigated in [41] by recording videos with a high-speed camera. Additionally, a new monitoring system that can show, within 2 s, the jetting status of a piezo-driven inkjet head was proposed in [42]. A low-cost and in-situ computational light beam field based droplet micro-sensing technique was studied for inkjet 3D printing quality assurance in [43]. Furthermore, a dual camera based catadioptric stereo system was proposed to measure the piezo self-sensing signals [44]. Based on the moinitoring process, a closed-loop control framework was presented by seamlessly integrating vision-based technique and neural network to inspect droplet behaviors and accordingly stabilize the printing process [45]. See [31] for a comprehensive review for monitoring devices in AM.

2.2. Machine learning methods for process monitoring in additive manufacturing

The instrumentation above enables the machine learning methods to perform the AM processes monitoring. As summarized in [46], machine learning facilitates the learning of fundamental knowledge on AM processes and provides actionable recommendations to optimize product quality. Here, we classify the machine learning methods into supervised, semi-supervised, and unsupervised approaches.

Supervised classification models were the most widely used approach for monitoring and anomaly identification. For instance, [22]

detected six kinds of layer-wise anomalies: recoater hopping, recoater streaking, debris, super-elevation, part failure, and incomplete spreading in LPBF via a convolution neural network (CNN) framework on video data. In [47], layer-wise visual inspection was performed, and a support vector machine (SVM) classifier was built for in-process part qualification. Other than the videos, [37] investigated the monitoring of SLM build quality using an acoustic emission sensor (fiber Bragg grating sensor) based on spectral CNN. Semi-supervised learning models were also used in scenarios where class labels are hard or expensive to be obtained. In [48], singular value decomposition (SVD) was used to extract features from photodiode measurements of LPBF, and a Gaussian mixture model was built for defect classification. Similarly, [26] used a semi-supervised CNN to monitor the average width and continuity in SLM based on process videos. A third category of the research falls into the unsupervised learning. In [49], powder bed images were analyzed to extract bag-of-words features and detect the six kinds of defects defined in [22]. As another example, [50] used selforganizing maps to identify the defects in the melt pool images of the directed energy deposition (DED) process. Recently, there is a growing area of research that uses multiple sensors' information and data fusion to perform process monitoring. For instance, [51] combined powder flow sensors, rake current, and rake positions in electron beam PBF systems for defect detection using SVM.

It is worth to mention that the machine learning methods have been applied broadly to monitor other engineering processes. Interested readers can refer to [52–54]. However, most of the current works conducted deep learning in a supervised manner, and this requires typically a well-defined ground-truth label, which is usually challenging to define clearly distinguishable ones. What is more, most current CNNs use static images as the study subject. The lack of temporal information limits its usage in the data, which requires feature understanding in the time domain. e.g., motion data. Therefore, in this paper, to investigate the droplet motion and its behavior evolution, the drop jetting video data are collected and studied using an unsupervised learning method.

3. Designed framework for printing process vision data learning

The proposed methodology for the unsupervised learning of the printing process video data is presented in Fig. 2. In this framework, firstly, the video data of the droplet jetting process are collected through two different methods: theoretical simulation and physical experiment, which are illustrated in the upper-left part of Fig. 2, the details will be introduced in Section 3.1. Then an unsupervised learning method DRNN (middle-left part of Fig. 2) is proposed to study the collected video data to understand the droplet evolution process, which will be introduced in Section 3.2. Experimental results and process dynamics understanding will be discussed in Section 4.

3.1. Simulation and experimental setup mechanism

In this section, two different types of videos of the droplet evolution process are collected. The first one is from simulation through the physical modeling method. The main reason to use the synthetic videos from the simulation is that the physical model is deterministic, and we have access to the underlying generative stimulus and all latent parameters. Thus we could attain a better understanding of the performance of the unsupervised learning method as well as the underlying knowledge the model learned from the synthetic videos. The second one is through experimental recording of the actual droplet jetting from a vision system in the inkjet printing process.

3.1.1. Synthetic data collection

For the synthetic videos, the droplet formation process is modeled by a computational fluid dynamics (CFD) model. The Navier–Stokes equations govern the physical model mass and momentum conservation for the liquid-gas interface, and it is assumed that the fluids are viscous,

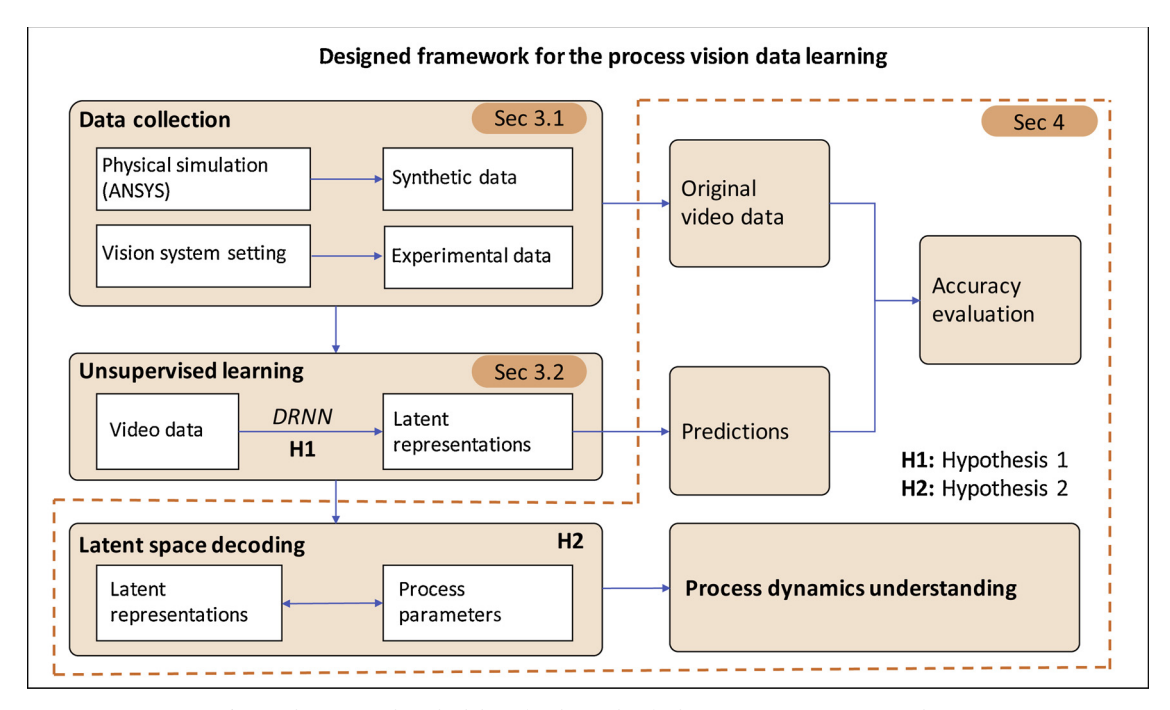


Fig. 2. The proposed methodology for the study of inkjet printing process vision data.

axisymmetric, and incompressible. The mass conservation condition is established by,

$$\nabla \cdot \mathbf{u} = 0 \tag{1}$$

where \mathbf{u} is the fluid velocity vector. Eq. (1) indicates that the amount of substance (ink) remains the same during the printing process. The momentum conservation, which is derived from the second Newton's law, is represented by,

$$\rho \left[\frac{\partial \mathbf{u}}{\partial t} + (\mathbf{u} \cdot \nabla) \mathbf{u} \right] = \nabla \sigma + f \tag{2}$$

where ρ is the density, $[\frac{\partial u}{\partial t}+(u\cdot\nabla)u]$ is the acceleration component, and $\nabla \sigma + f$ is the total force that entails shear stress ($\nabla \sigma$) and other external forces (f). $\nabla \sigma$ can be divided into pressure related and viscosity related componets, which are represented as $-\nabla p$ and $\mu \nabla^2 \mathbf{u}$, respectively. Thus, Eq. (2) can be rewritten $\frac{\partial \hat{\mathbf{u}}}{\partial t} = -(\mathbf{u} \cdot \nabla)\mathbf{u} + \mu \nabla^2 \mathbf{u} - \nabla p + f$. For specific circumstances, Eqs. (1) and (2) can be derived into different coordinate systems. The continuous equations are usually turned into stepped discrete form, which is widely applied by commercial tools. Physical properties such as density and viscosity follow the rule of volume fraction shown in Eqs. (3) and 4)) [55-57], which is important because the material to be printed usually has multiple components.

$$\rho = f\rho_1 + (1 - f)\rho_2 \tag{3}$$

$$\mu = \frac{f\rho_1 \mu_1 + (1 - f)\rho_1 \mu_2}{\rho} \tag{4}$$

The constitutive model that describes the inkjet droplet formation process is solved in ANSYS-Fluent. To start, the geometry of the nozzle is defined, specifically the nozzle diameter ($50 \, \mu m$). The inner part of the printhead solution/ink undergoes a wave propagation induced by the piezoelectric actuation that can be modeled using acoustics [58], which is out of the scope of this work. This piezoelectric actuation will determine the initial velocity of the droplet (see Fig. 1), which is defined as a trapezoidal signal (see Fig. 3) in ANSYS-Fluent. Fig. 3 shows the specific rise time (t_R), dwell time (t_D), and fall time (t_F) used to solve the problem. Particularly, this waveform is read by ANSYS-Fluent to mimic the piezoelectric actuation, hence giving the droplets' initial velocity. For the simulations, a pressure-based solver is used. The mass

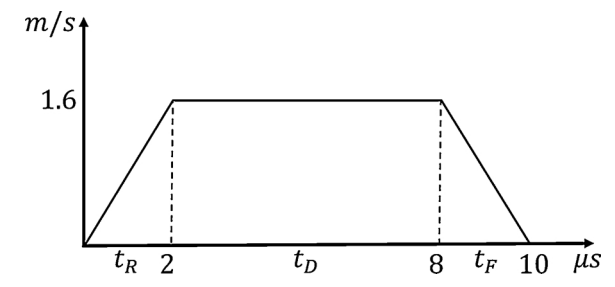


Fig. 3. User defined input velocity profile in the simulations.

conservation of the velocity field is obtained by solving a pressure equation, which is derived from the mass continuity and momentum conservation equations [59]. Additionally, the volume-of-fluid (VOF) approach, which allows to track the shape and position of the droplets, is utilized in ANSYS-Fluent. In order to solve the pressure-velocity coupling problem, we use a fractional step scheme, least squares cell-based gradient evaluation, pressure staggering option scheme, and QUICK scheme for quadrilateral and hexahedral meshes. Finally, ANSYS-Fluent permits to create materials with various physical properties (i.e., density, viscosity, surface tension, etc.), thus several solution/inks are used for the simulations.

Once the geometry, initial velocity, solver, and material properties are specified, a journal file is created from ANSYS-Fluent. This file is utilized to customize the material properties (see Table 1) of the solution/inks and to automate the commands for recursive simulations. The simulations are run by setting the number of cores with 4*cores*, the time step size with $9e^{-08}s$, number of time steps with 1200steps, the contact angle with 90° , and the nozzle diameter with $50 \, \mu m$. Additionally,

Table 1Ranges of the solution/ink properties for video generation.

Material properties	Low level	High level
Density (kg/m³) Viscosity (kg/m.s) Surface tension (dyn/cm)	800 0.0005 50	8000 0.15 80

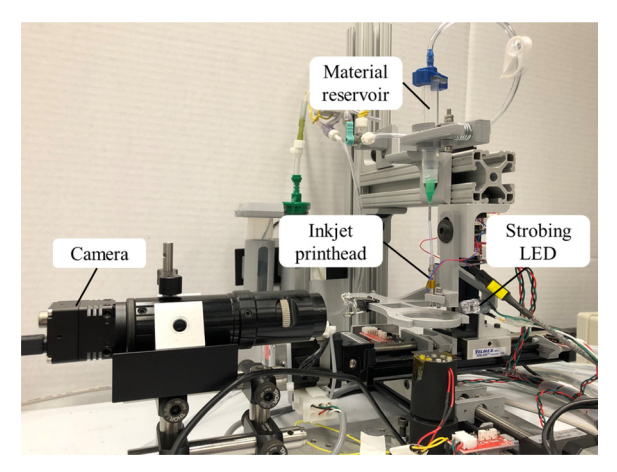


Fig. 4. Inkjet printing devices and data collection system.

different solution/ink properties, as shown in Table 1, are utilized for the design of experiments (DOE), and then simulations are performed for each case. Therefore, the synthetic videos are generated. In particular, simulations are performed based on Latin hypercube design using min-max criterion [60].

As a result, each video in the synthetic dataset has a unique set of stimulus parameters, as described in Table 1. For each video, the droplet formation process, from the head of the nozzle to the substrate, is simulated. Since different types of droplet behaviors reflect various printability modes, the flow pattern of the flying droplet can be used to infer the printing quality in the PIJ process.

3.1.2. Experimental data collection

The hardware of our video collection system is shown in Fig. 4. In this system, a piezo-based micro-dispensing nozzle (MicroFab Inc.) is used as the inkjet print-head with typical Newtonian liquid to generate droplets, it has a nozzle size of $50\,\mu m$, and the jetting rate can vary from 100 to 1000 droplets per second. A CCD camera (Sensor Technologies Inc.) coupled with magnification lens works as the video capturing device in this system. The video resolution in use is 640×480 pixels. To collect videos of droplet generation process, strobing technology is also known as synchronized illumination is utilized [61], by tuning the delay time between the jetting signal and lighting signal of the LED for illumination, the time between every two frames of the collected video

can be set precisely. In the data collection, this time is fixed to $20\,\mu s$. In this paper, 4K experimental videos are collected for the learning framework.

3.2. Unsupervised learning of the process vision data

Through the aforementioned two data-collection approaches, the video of drop ejecting from the nozzle head to the substrate can be collected. Based on these process vision data, we proposed to use an unsupervised learning method, DRNN, to study such data. Based on the observation of the successful unsupervised learning methods in the existing studies [62,63] and the fact that the drop-flow video has a spatio-temporal structure, we have the following two hypotheses.

Hypothesis 1 (H1). With DRNN, a latent representation of the video data can be learned, and such representation can be used for reproducing the original data.

Hypothesis 1 (H2). Through latent space decoding, the learned representation can be related to the droplet evolution stimulus parameters and further supports process dynamics understanding.

As illustrated in the middle part of Fig. 2, if the (H1) is valid, then based on the learned latent representation, a reproduction of original data can be mapped from this representation, i.e., a prediction can be made. By estimating the difference between the original data and the predictions, we could evaluate the performance of the proposed DRNN. To test this hypothesis, a PredNet is used to implement the DRNN. The concept of the PredNet is presented in Fig. 5.

In this DRNN framework, the study subject is the video data of the printing process. Here, for the sake of simplicity, we represent it in an image sequence format. Each video consists of a serial of image frames in the time domain, i.e., the input of DRNN is a sequence of image frames (x_t) . Then the input frame sequences pass through a recurrent neural network (RNN), as shown in Fig. 5. The RNN mainly includes four blocks (four type of neurons in the network) in the architecture, a recurrent representation layer R_t^l , a prediction neuron \hat{I}_t^l , an input neuron I_t^l and an error neuron E_t^l , where l is the layer of RNN (l=1,...,L). In each layer at time t, based on the recurrent neuron R_t^l , we could obtain the predictions \hat{I}_t^l , then the predictions are compared with the input neuron I_t^l correspondingly, an error neuron can be calculated through the comparison. For the input neuron, the lowest layer is set as the actual image frame, i.e., $I_t^0 = x_t$. As can be seen from Fig. 5 the recurrent neuron R_t^l is calculated according to the upper layer recurrent

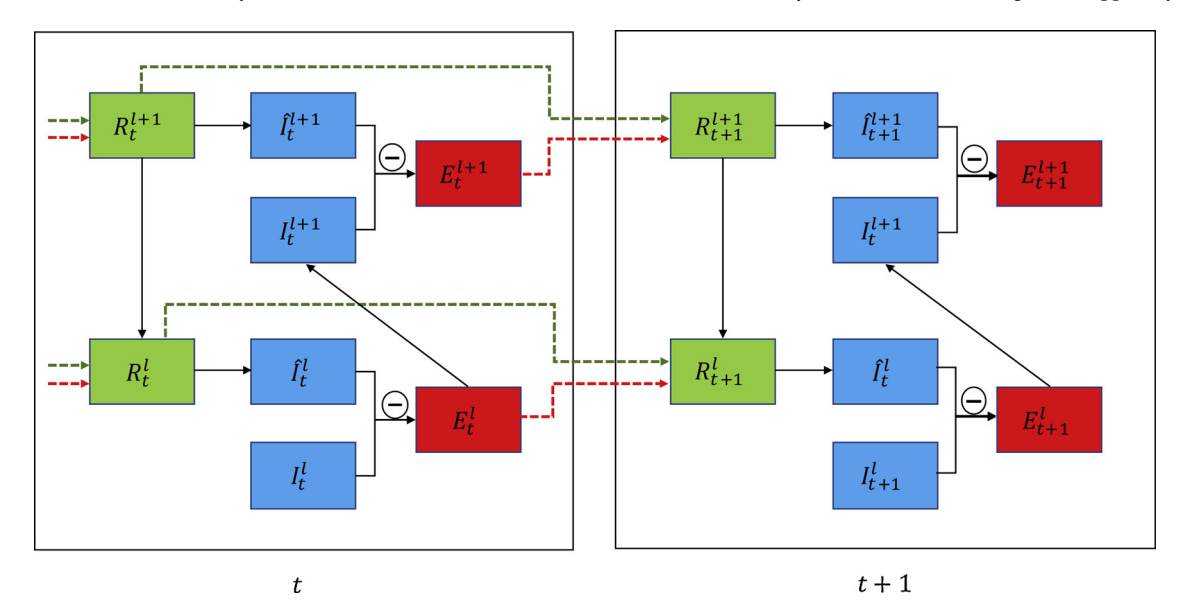


Fig. 5. The deep recurrent neural network structure used for the printing process video learning, the concept is credited to [27].

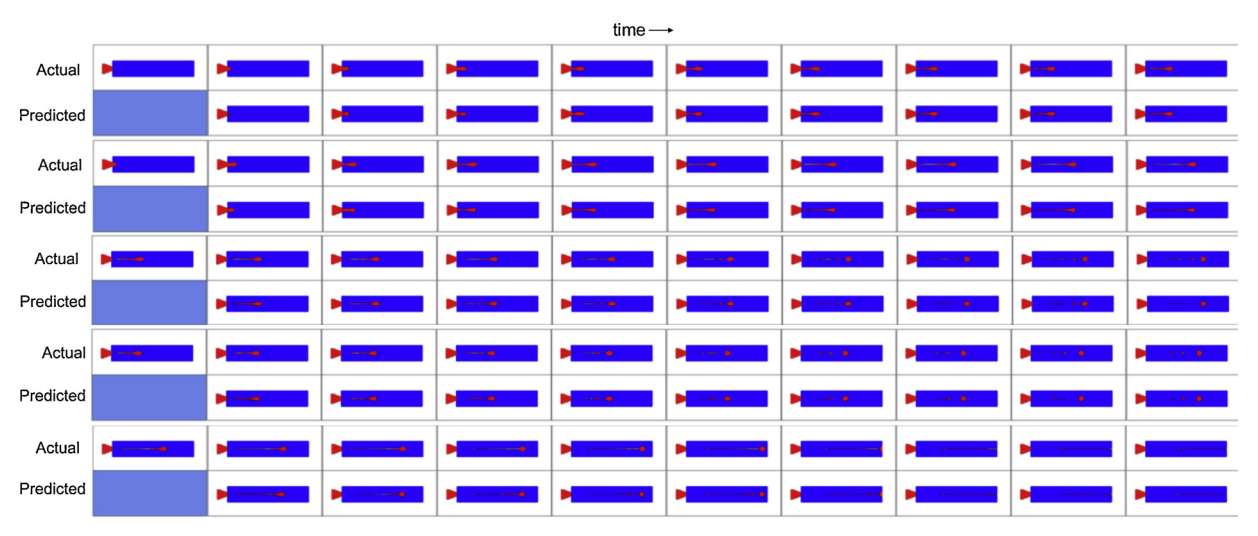


Fig. 6. One-step-ahead prediction results of the frame sequences in droplet forming process videos.

neuron R_{t-1}^{l+1} , last time frame recurrent neuron and the error neuron, R_{t-1}^{l} and E_{t-1}^{l} . Specifically, a convolutional LSTM operation [27,64] is used to update the recurrent neuron.

$$R_{t}^{l} = \begin{cases} \text{ConvLSTM}(R_{t-1}^{l}, E_{t-1}^{l}) & \text{if } l = L\\ \text{ConvLSTM}(R_{t-1}^{l}, E_{t-1}^{l}, \text{UpSample}(R_{t}^{l+1})) & 0 \le l < L \end{cases}$$
(5)

where R_0^l , E_0^l are initialized as ${\bf 0}$. Based on the recurrent neuron, the prediction one is computed by using the general convolution operation in deep learning.

$$\widehat{I}_t^l = \text{Relu}(\text{Conv}(R_t^l)) \tag{6}$$

With the prediction neuron, the error can be calculated by comparing it to the input neuron. Here the error is split into ReLU-activated positive and negative prediction errors, and then are concatenated to match with the feature dimension [27].

$$E_t^l = [\text{Relu}(I_t^l - \widehat{I}_t^l); \text{Relu}(\text{Relu}(\widehat{I}_t^l - I_t^l)]$$
(7)

The error neuron is then used to compute the input neuron in upper layer, also using the general convolution and pooling operation in deep learning.

$$I_t^l = \begin{cases} \text{MaxPool}(\text{Relu}(\text{Conv}(E_{t-1}^l))) & 0 < l \le L \\ x_t & l = 0 \end{cases}$$
(8)

According to the update rules of each blocks in the network architecture, we train the image sequences with a loss function ℓ_{train} . Here the loss function is to minimize the total weighted error neurons (E_t^L) , the weight depends on the time step (w_t) and the layer (w_l) .

$$\ell_{\text{train}} = \sum_{t} w_t \sum_{l} \frac{w_l}{n_l} \sum_{n_l} E_t^l \tag{9}$$

where n_l is the number of neurons in the lth layer.

Based on the DRNN discussed above, we can see that a representation layer is used for the RNN, which can be seen as a latent representation of each frame in different time standpoints. To verify the second hypothesis, (H2), such representation layer is decoded, and its relation with process governing parameters such as material property is investigated. A detailed discussion on experimental validation will be presented in the next section.

4. Experimental results and discussion

4.1. Synthetic video prediction results

To investigate the performance of the proposed in-situ video

learning framework and understand what the representations of the RNN learned, we firstly used the simulation method to generate synthetic videos of the droplet forming process of the inkjet printing process. We have access to all of the parameters and the stimulus mechanism for the video synthesis. Comparing to the experimental videos, which usually includes several types of uncertainty such as humidity and slight vibrations, the pure simulation videos could help us gain a well understanding of what the proposed method have learned and how the learned representations related to the printing process stimulus. Here, the droplet forming video was generated through the CFD model. By solving the constitutive model that describes the inkjet droplet formation process in ANSYS, a set of image sequences based on finite element analysis (FEA) can be generated. In each sequence, ten consecutive image frames are sampled for each video. The image pixel size are 128×320 . In this experiment, 10 K sequences are used for training and 800 for both validation and testing. As regards the network parameters settings, the RNN has four layers (L = 4) in the architecture. In all of the convolution operation, the filter size is set as 3×3 , and the max-pooling stride is 2. The number of filters (channels) used for R^{l} and I^{l} are both set as (3, 48, 96, 192). The loss function is optimized using the Adam algorithm with learning rate of 0.001 and $\beta_1 = 0.9$, $\beta_2 = 0.999$ [65].

In the first experiment, we use the one-step-ahead prediction pattern when training the frame sequences, i.e., the network is predicting the next frame based on the previous and the current frame. The predicted results are presented in Fig. 6. 1.0,0.0,0.0 In this Figure, the model is always predicting one step frame ahead from the current frames. It can be observed that the first frame is uniform, mainly because the representation neurons are initialized with $\boldsymbol{0}$. Without temporal information incurred, the second predicted frames are approximations of the first frames, as can be seen from the second column of the predicted frames in Fig. 6. Furthermore, with information of more time steps, the model can learn an approximate representation of the underlying dynamics and predict accurate frames as shown in the later columns of predicted results in Fig. 6.

To quantitatively evaluate the performance of the learning method, here two metrics, mean-squared error (MSE) and structure similarity index measure (SSIM) [66], are applied to describe the accuracy of the prediction method. SSIM is a perceptual metric that quantifies image quality degradation caused by processing such as data compression or by losses in data transmission, a larger SSIM indicates better similarity, with the range of [-1,1]. Here we compared the proposed method with a trivial solution that is directly copying the last frame. For the training loss function, to investigate the different weights and their prediction performances, here two settings as suggested in [27] are used. The first

Table 2Performance comparison of the one-step ahead prediction methods.

	MSE	SSIM
Copy last frame ℓ_1 ℓ_2	2.375×10^{-3} 0.422×10^{-3} 0.487×10^{-3}	0.642 0.967 0.951

one uses loss only concentrating on the lowest layer, i.e., $w^0 = 1$, $w^{l>0} = 0$ and denoted as ℓ_1 , while the other one is also concentrating on the lowest layer but enforcing moderate weights on upper layers, $w^0 = 1$, $w^{l>0} = 0.1$ and denote as ℓ_2 , the time step weights are set as $w_0 = 0$, $w_{t>0} = 1$. The comparison result of three methods on the testing data set is shown as in Table 2, the metrics are calculated through averaging all of the predictions after the first time step.

It can be seen from Table 2 that the MSE of the proposed method is much smaller than simply copying the last frame while has a higher SSIM. Besides, we can observe that the training loss focus on the lowest layer performs slightly better than the one with weights of training loss lightly spread on upper layers. All of these experiments reveal that the proposed method can learn a latent representation of video data, which can be used for the predictions of the droplet evolution in the inkjet printing process. To this end, the first hypothesis, (H1), is validated.

4.2. Multi-step prediction of the video data

In Section 4.1, we can see that the proposed unsupervised learning method can accurately predict the droplet frames in one time-step ahead. In practice, it is usually expected a prediction method can predict a 'long-term' results since a long-term prediction in the monitoring can provide us enough buffer for timely process correction if there is any anomaly. In order to investigate the extrapolation capability of the proposed method, we conduct a multi-step droplet jetting behavior prediction experiment in this section.

To conduct the multi-step prediction, a natural way is to feed the network with predicted frames instead of the actual images under the one step ahead prediction architecture. Considering the network need to take the actual image frames as input to learn the underlying dynamics. Therefore, for multi-step prediction, the first few image frames are using the same principle as the one-step-ahead prediction, while in the following time step, the predicted frames are fed into the network as actual input. In the experiment, 15 image frames are used for the training with the first ten actual image input and the last five frames as recursively predicting (denoted as ℓ_{t+5}). With the same network setting as in Section 4.1, we train the network with 15 frames. Regarding the first ten images, the error between the actual image and predicted one is calculated through Eq. (7), while the last five are using the mean absolute error. The reason is we only consider the difference between the actual frames and predicted ones rather than the positive/negative divergence as we feed the predictions as the input. The prediction results are presented as in Fig. 7.

It can be observed from Fig. 7 with one time ahead prediction (ℓ_{t+1}) method, the model is reasonably accurate at the beginning (t+2), however, with time increasing, the predictions naturally breakdown since there is no information to guide the model to learn the underlying dynamics. Nevertheless, with the ℓ_{t+5} method, we can see the model still can predict the droplet jetting behavior. For example, in the first and second sequence, ℓ_{t+5} can predict the same pinching position, while the ℓ_{t+1} method predicts a result close to the last seen frame. Similarly, in the last sequence, the ℓ_{t+5} can predict the similar pinching behavior (pinching position and type) with the actual case, but the ℓ_{t+1} can only predict an extension of the last seen frame. From this experiment, we can see that with the adjustment of the training loss for multistep prediction, and the model exhibits better extrapolation capability. For a quantitative comparison, the MSE of the predictions from

different methods is shown in Fig. 8.

From Fig. 8, we can see that the MSE of ℓ_{t+5} increases almost linearly for 2-10 time steps ahead extrapolation, although our model is only trained with t+5 prediction. While the ℓ_{t+5} increased almost twice larger than ℓ_{t+1} . It reveals that with the fine-tuning of the training loss function, the proposed method can make multi-step predictions.

4.3. Latent variable decoding

From the prediction experiments, the results show that the DRNN can adapt to the underlying dynamics of the droplet forming process. To investigate how the network learns such representations of the dynamics, we conduct a decoding experiment. As mentioned in Section 4.1, the synthetic videos are generated through FEA simulation. In the simulation videos, three governing parameters, material properties, density (ρ), viscosity (μ), and surface tension (γ), are selected to create the simulation video. Thus, the latent parameters of the video data consist of these three parameters. To understand what the trained model learned from the data, we decode the latent parameters from the representation neurons (R^l) in different layers by using lasso regression. In this regression experiment, the representation neurons in the second and third-time steps, i.e., R_2^l and R_3^l , are selected. To verify the decoding performance, a partial data are randomly selected from the whole dataset to extract the implicit information embedded in the representation neurons of these samples. Hence, the regression is conducted on 3K training sequences, 1K validation, and testing sequences, respectively. To reveal the effectiveness of the proposed method, an untrained network with random initial weights is also used in the decoding experiment to compare with ℓ_1 and ℓ_2 networks.

The decoding accuracy comparison results are presented in Fig. 9. Several interesting patterns can be observed from the decoding experiment. Firstly we can see with randomly initialized weights in the network, the network still can obtain a good decoding accuracy for the viscosity and surface tension parameter. This is mainly because of the central limit theorem, with the large number of randomized weights in the network, it is expected to have the above chance of decoding performance [67]. Secondly, the proposed network with two different weights settings, ℓ_1 and ℓ_2 , achieves very close decoding results for all of the three parameters, the ℓ_1 decodes slightly better than ℓ_2 on density and surface tension. The ℓ_2 decodes slightly better than ℓ_1 on viscosity. Lastly, the representations of different layers reveals that the proposed network can obtain a good decoding accuracy of the three parameters after the first layer. This suggests that the representation neurons can adapt to the original data very fast from the first layer, as layer increases, the network can learn the pattern more closely to the original data. From the above experiments, we can see that the proposed method can relate the learned latent representations to the process parameters, which verified the second hypothesis (H2).

4.4. In-situ PIJ video prediction and physical parameters decoding

From the previous sections, we can see that the DRNN has an implicit learning capability to understand the motion of the droplet and its transformation undergoing on the synthetic videos. To test its performance on the real data in the actual printing process, we collected 4K sequences of the droplet forming process for training through the system in Section 3.1.2. Here we mainly used the water and ethanol as the testing materials in the experiment system. In this experiment, one material is used to record the droplet jetting behavior, and two major physical parameters are controlled in process, i.e., the air pressure, and driving voltage. The image frames sampled from the video are cropped and down-sampled to 128×160 pixels. Similarly, for the hyper-parameters setting in the network, ten consecutive image frames are sampled for each video in each sequence. In this experiment, 4K sequences are used for training and 500 for both validation and testing. As regards the network parameters settings, the DRNN has five layers (L=5) in

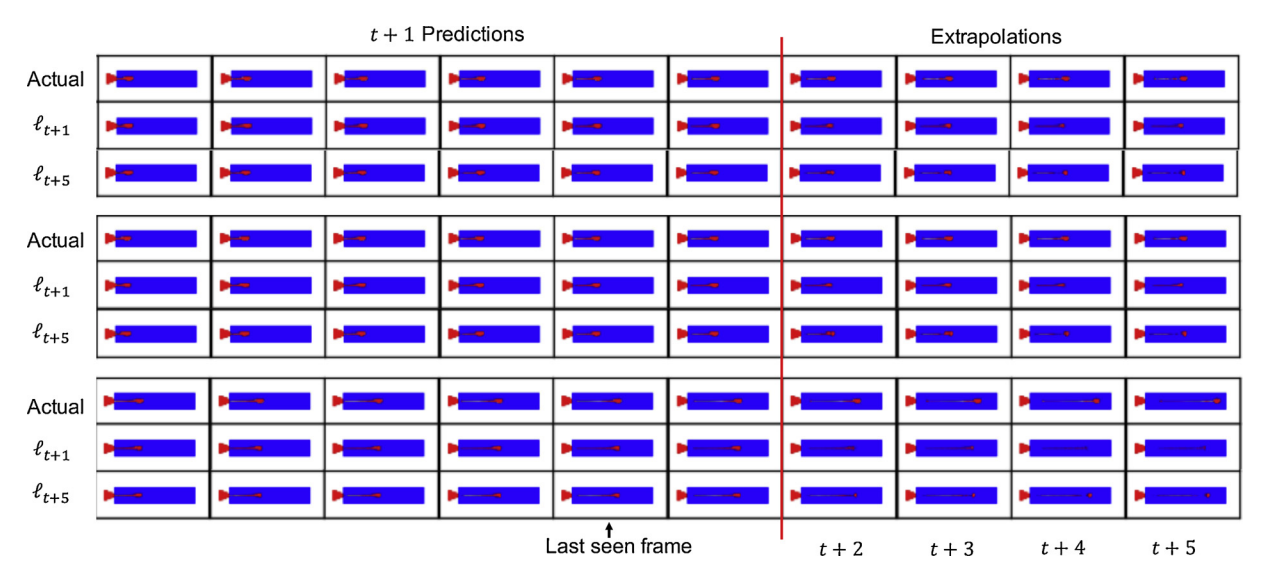


Fig. 7. Muti-step prediction of the droplet jetting behavior of the PIJ process.

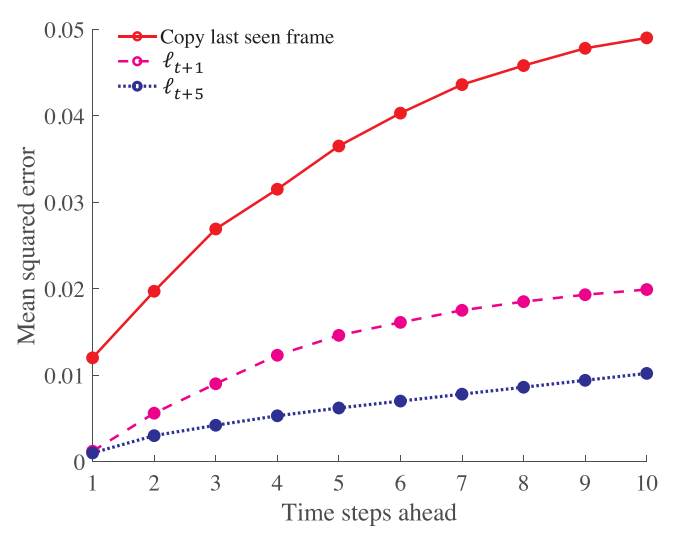


Fig. 8. MSE comparison of multi-step prediction methods.

the architecture. In all of the convolution operation, the filter sizes are set as 3×3 , and the max-pooling stride is 2. The number of filters (channels) used for R^l and I^l are both set as (1, 32, 64, 128, 256). The loss function is again optimized with the Adam algorithm with default parameters. The learning rate will be decreased to 0.0001 during the midpoint of the training.

Sample predictions (loss function ℓ_2) are presented as in Fig. 10. We

can see that the proposed DRNN has an accurate prediction for the droplet jetting behaviors. It can be observed that as the time progresses, the network can adapt to the droplet forming dynamics. At the fourth and fifth steps, the network can only predict a blur representation of the droplet. This is mainly because the droplet is not pinched from the nozzle in the first few time steps, but after the fifth step, the network can predict certain behavior of the droplet jetting. Besides, the network can predict different pinch behaviors. For example, in the second sequence and third sequence, the droplet forms into two different types, one is becoming satellites, and another one is clearly pinched with one droplet. Nevertheless the network can perform a good forecasting, although the droplet in this two sequences are very similar in previous steps. Again, this experiment validated the proposed hypothesis (H1) in Section 3.2.

To quantitatively compare the prediction methods, the same metrics mentioned in Section 4.1 are used, the comparison results are shown in Table 3. From the table, we can see the network with training loss function ℓ_2 achieves the best performance on the real experimental data. This reveals that for different tasks, the network performs differently with different optimal parameters.

To understand the learned representation, we decode the latent parameters and apply them to estimate the air pressure and voltage in the actual printing process. Here we use 1K recorded sequences in this experiment, then fit a linear fully-connected layer on the learned representation to estimate the air pressure and voltage of the printing process. The representation neurons (R^l) in 10th time step are used. Similarly, an untrained network with random initial weights is also used to compare with two training loss settings. The estimation results

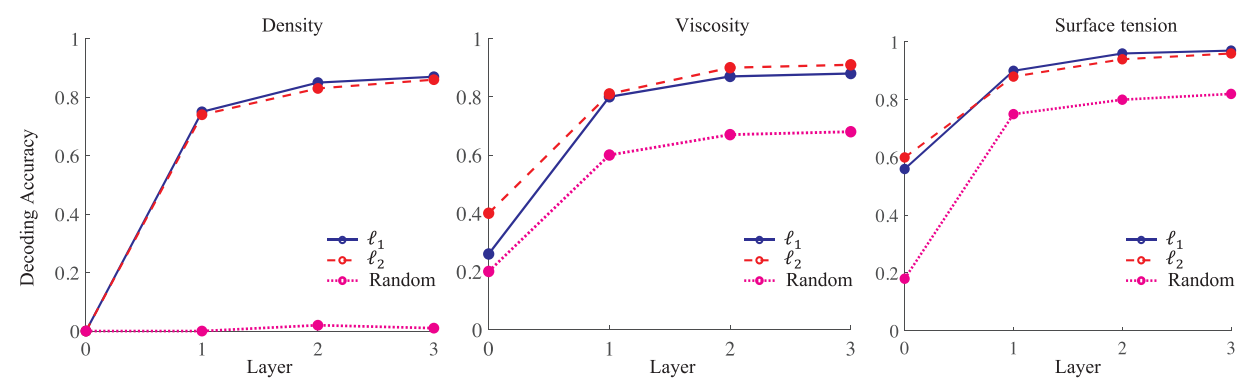


Fig. 9. Decoding accuracy of latent parameters with different weights settings in the networks.

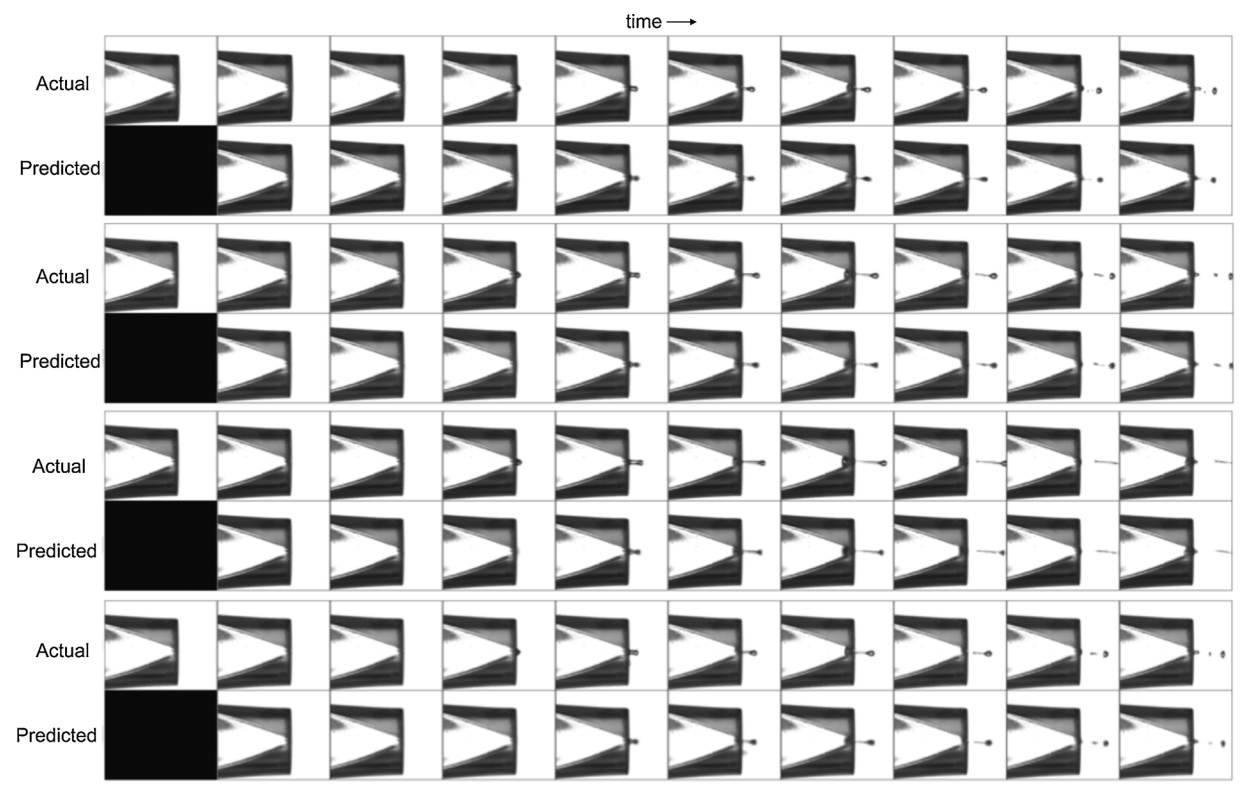


Fig. 10. Prediction of the droplet jetting behavior in actual printing process.

Table 3Metrics comparison with different prediction methods.

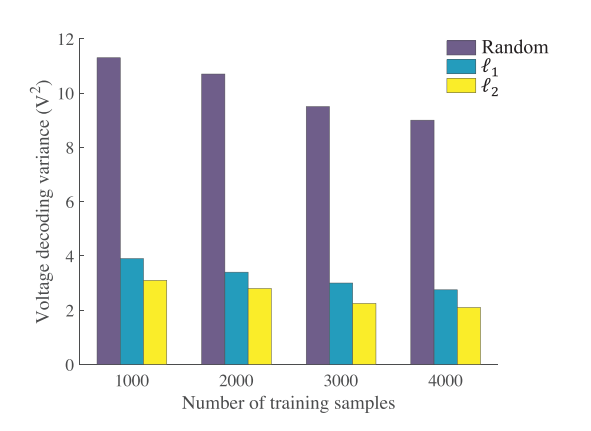
	MSE	SSIM
Copy last frame	0.2073 0.0238	0.678 0.845
$oldsymbol{\ell}_1 \ oldsymbol{\ell}_2$	0.0238	0.862

are shown in Fig. 11. We can see that with 1K training samples, the learned representation from DRNN with ℓ_1 can outperform 65.4% and 69.5% better than the network with randomized weights when explaining the voltage and pressure parameters respectively. With 4K training samples, we can see that the ℓ_1 can achieve the estimation variance of 2.1 V^2 and 1.05(inH2O) 2 for the voltage and pressure (in inch of water). All of these experiments suggest that the proposed unsupervised learning framework can learn a meaningful representation in latent space, which is helpful for the understanding of droplet dynamics and physical parameters estimation. This supports the

hypothesis, as described in (H2). It should be noted that our system could be capable of using any other liquid materials. Here we mainly used two materials to collect the vision data of the system, and this paper we primarily focused on the data analytic of the process video. It can be extended to any similar materials and process vision data.

5. Conclusion

In this paper, an unsupervised learning framework for the vision data of the inkjet printing process is proposed for the understanding of the drop flow pattern of the inkjet printing process and the underlying dynamics. Two hypotheses are proposed in the learning framework. To verify these hypotheses, two data collecting approaches are used for the collection of both simulation and experimental data. The proposed method is trained with the process video data of the droplet evolution in the inkjet printing process. Experimental results validate the proposed hypotheses, i.e., the DRNN can learn a latent representation of the video data, which can be used for the droplet behavior prediction.



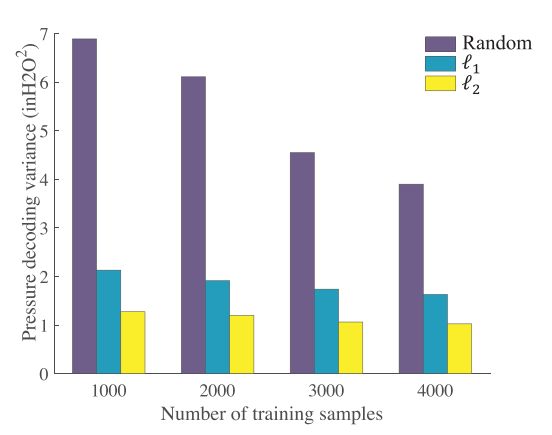


Fig. 11. Parameters estimation accuracy.

To understand what the network learned, the latent representation is decoded and used for correlating to the process governing stimulus. The experimental results demonstrate that the DRNN can learn the motion of the droplet and its forming process, which is useful for the jetting behavior prediction and supports physical parameters estimation. With such capabilities, the proposed framework can be further used in the real-time monitoring of the inkjet printing process. 1.0,0.0,0.0 There are several limitations of this work. First, the explicit relation between the learned representation and droplet behavior is not investigated. Second, how to utilize the learned features for process parameter adjustment is not studied. Hence, further work is mainly of two folds. The first one is to integrate the learned latent representation with high prediction efficiency of droplet behavior in additive manufacturing. With such a fast prediction method, the anomaly of the droplet and printability can be predicted in advance. Since the method has such prognostic capability, the second one is to incorporate it into the in-situ real-time monitoring and process control to improve the printing quality of the inkjet process.

Conflicts of interest

The authors declare no conflicts of interest.

Acknowledgement

We acknowledge the support from the National Science Foundation (NSF) through CMMI-1846863 and the seed fund support from SMART. We thank the support provided by the Center for Computational Research at the University at Buffalo.

References

- M. Singh, H.M. Haverinen, P. Dhagat, G.E. Jabbour, Inkjet printing-process and its applications, Adv. Mater. 22 (6) (2010) 673–685.
- [2] J. Sun, B. Bao, M. He, H. Zhou, Y. Song, Recent advances in controlling the depositing morphologies of inkjet droplets, ACS Appl. Mater. Interfaces 7 (51) (2015) 28086–28099.
- [3] V. Mironov, T. Boland, T. Trusk, G. Forgacs, R.R. Markwald, Organ printing: computer-aided jet-based 3d tissue engineering, Trends Biotechnol. 21 (4) (2003) 157–161.
- [4] H. Sirringhaus, T. Kawase, R. Friend, T. Shimoda, M. Inbasekaran, W. Wu, E. Woo, High-resolution inkjet printing of all-polymer transistor circuits, Science 290 (5499) (2000) 2123–2126
- [5] P. Yan, E. Brown, Q. Su, J. Li, J. Wang, C. Xu, C. Zhou, D. Lin, 3d printing hierarchical silver nanowire aerogel with highly compressive resilience and tensile elongation through tunable poisson's ratio, Small 13 (38) (2017) 1701756.
- [6] J.-U. Park, S. Lee, S. Unarunotai, Y. Sun, S. Dunham, T. Song, P.M. Ferreira, A.G. Alleyene, U. Paik, J.A. Rogers, Nanoscale, electrified liquid jets for high-resolution printing of charge, Nano Lett. 10 (2) (2010) 584–591.
- [7] E. Tekin, P.J. Smith, U.S. Schubert, Inkjet printing as a deposition and patterning tool for polymers and inorganic particles, Soft Matter 4 (4) (2008) 703–713.
- [8] D. Pesach, A. Marmur, Marangoni effects in the spreading of liquid mixtures on a solid, Langmuir 3 (4) (1987) 519–524.
- [9] S.D. Hoath, Fundamentals of Inkjet Printing: the Science of Inkjet and Droplets, John Wiley & Sons, 2016.
- [10] H. Wijshoff, The dynamics of the piezo inkjet printhead operation, Phys. Rep. 491 (4–5) (2010) 77–177.
- [11] O.A. Basaran, H. Gao, P.P. Bhat, Nonstandard inkjets, Annu. Rev. Fluid Mech. 45 (2013) 85–113.
- [12] D. Bartolo, A. Boudaoud, G. Narcy, D. Bonn, Dynamics of non-newtonian droplets, Phys. Rev. Lett. 99 (17) (2007) 174502.
- [13] E.K. Hill, R.L. Watson, D.E. Dunstan, Rheofluorescence technique for the study of dilute meh-ppv solutions in couette flow, J. Fluoresc. 15 (3) (2005) 255–266.
 [14] M. Tsai, W.-S. Hwang, H. Chou, P. Hsieh, Effects of pulse voltage on inkjet printing
- of a silver nanopowder suspension, Nanotechnology 19 (33) (2008) 335304.
- [15] K. Barton, S. Mishra, A. Alleyne, P. Ferreira, J. Rogers, Control of high-resolution electrohydrodynamic jet printing, Control Eng. Pract. 19 (11) (2011) 1266–1273.
- [16] P.K. Rao, J.P. Liu, D. Roberson, Z.J. Kong, C. Williams, Online real-time quality monitoring in additive manufacturing processes using heterogeneous sensors, J. Manuf. Sci. Eng. 137 (6) (2015) 61007.
- [17] H. Dong, W.W. Carr, J.F. Morris, Visualization of drop-on-demand inkjet: drop formation and deposition, Rev. Sci. Instrum. 77 (8) (2006) 85101.
- [18] H. Qin, X. Zhang, R. Singh, Z. Zhang, Y. Chen, In-process monitoring of electrohydrodynamic inkjet printing using machine vision, AIP Conference Proceedings, Vol. 2102 (2019) 70008.
- [19] C. Xu, Z. Zhang, J. Fu, Y. Huang, Study of pinch-off locations during drop-on-

- demand inkjet printing of viscoelastic alginate solutions, Langmuir 33 (20) (2017) 5037–5045.
- [20] D. Wu, C. Xu, Predictive modeling of droplet formation processes in inkjet-based bioprinting, J. Manuf. Sci. Eng. 140 (10) (2018).
- [21] C. Gobert, E.W. Reutzel, J. Petrich, A.R. Nassar, S. Phoha, Application of supervised machine learning for defect detection during metallic powder bed fusion additive manufacturing using high resolution imaging, Addit. Manuf. 21 (2018) 517–528.
- [22] L. Scime, J. Beuth, A multi-scale convolutional neural network for autonomous anomaly detection and classification in a laser powder bed fusion additive manufacturing process, Addit. Manuf. 24 (2018) 273–286.
- [23] R.C. O'Reilly, D. Wyatte, J. Rohrlich, Learning Through Time in the Thalamocortical Loops, (2014) (arXiv preprint), arXiv:1407.3432.
- [24] R. Goroshin, J. Bruna, J. Tompson, D. Eigen, Y. LeCun, Unsupervised learning of spatiotemporally coherent metrics, Proceedings of the IEEE International Conference on Computer Vision (2015) 4086–4093.
- [25] L. Scime, J. Beuth, Anomaly detection and classification in a laser powder bed additive manufacturing process using a trained computer vision algorithm, Addit. Manuf. 19 (2018) 114–126.
- [26] B. Yuan, B. Giera, G. Guss, I. Matthews, S. Mcmains, Semi-supervised convolutional neural networks for in-situ video monitoring of selective laser melting, 2019 IEEE Winter Conference on Applications of Computer Vision (WACV), IEEE, 2019, pp. 744–753
- [27] W. Lotter, G. Kreiman, D. Cox, Deep Predictive Coding Networks for Video Prediction and Unsupervised Learning, (2016) (arXiv preprint), arXiv:1605.08104.
- [28] R.P. Rao, D.H. Ballard, Predictive coding in the visual cortex: a functional interpretation of some extra-classical receptive-field effects, Nat. Neurosci. 2 (1) (1900) 70
- [29] A. Clark, Whatever next?. Predictive brains, situated agents, and the future of cognitive science, Behav. Brain Sci. 36 (3) (2013) 181–204.
- [30] R. Chalasani, J.C. Principe, Deep Predictive Coding Networks, (2013) (arXiv preprint), arXiv:1301.3541.
- [31] S.K. Everton, M. Hirsch, P. Stravroulakis, R.K. Leach, A.T. Clare, Review of in-situ process monitoring and in-situ metrology for metal additive manufacturing, Mater. Des. 95 (2016) 431–445.
- [32] G. Tapia, A. Elwany, A review on process monitoring and control in metal-based additive manufacturing, J. Manuf. Sci. Eng. 136 (6) (2014) 60801.
- [33] M. Grasso, B.M. Colosimo, Process defects and in situ monitoring methods in metal powder bed fusion: a review, Meas. Sci. Technol. 28 (4) (2017) 44005.
- [34] H. Sun, P.K. Rao, Z.J. Kong, X. Deng, R. Jin, Functional quantitative and qualitative models for quality modeling in a fused deposition modeling process, IEEE Trans. Autom. Sci. Eng. 15 (1) (2017) 393–403.
- [35] B. Lane, S. Moylan, E.P. Whitenton, L. Ma, Thermographic measurements of the commercial laser powder bed fusion process at nist, Rapid Prototyp. J. 22 (5) (2016) 778–787.
- [36] U.S. Bertoli, G. Guss, S. Wu, M.J. Matthews, J.M. Schoenung, In-situ characterization of laser-powder interaction and cooling rates through high-speed imaging of powder bed fusion additive manufacturing, Mater. Des. 135 (2017) 385–396.
- [37] S.A. Shevchik, C. Kenel, C. Leinenbach, K. Wasmer, Acoustic emission for in situ quality monitoring in additive manufacturing using spectral convolutional neural networks. Addit. Manuf. 21 (2018) 598–604.
- [38] J.A. Kanko, A.P. Sibley, J.M. Fraser, In situ morphology-based defect detection of selective laser melting through inline coherent imaging, J. Mater. Process. Technol. 231 (2016) 488–500
- [39] Z. Wang, E. Denlinger, P. Michaleris, A.D. Stoica, D. Ma, A.M. Beese, Residual stress mapping in inconel 625 fabricated through additive manufacturing: method for neutron diffraction measurements to validate thermomechanical model predictions, Mater. Des. 113 (2017) 169–177.
- [40] P. Sitthi-Amorn, J.E. Ramos, Y. Wangy, J. Kwan, J. Lan, W. Wang, W. Matusik, Multifab: a machine vision assisted platform for multi-material 3d printing, ACM Trans. Graph. (TOG) 34 (4) (2015) 129.
- [41] H. Yang, Y. He, C. Tuck, R. Wildman, R. Hague, High viscosity jetting system for 3d reactive inkjet printing, Twenty Forth Annual International Solid Freeform Fabrication Symposium – An Additive Manufacturing Conference (2013) 505–513.
- [42] K.-S. Kwon, Y.-S. Choi, D.-Y. Lee, J.-S. Kim, D.-S. Kim, Low-cost and high speed monitoring system for a multi-nozzle piezo inkjet head, Sens. Actuators A: Phys. 180 (2012) 154–165.
- [43] A. Wang, T. Wang, C. Zhou, W. Xu, Luban:, Low-cost and in-situ droplet microsensing for inkjet 3d printing quality assurance, Proceedings of the 15th ACM Conference on Embedded Network Sensor Systems (2017) 27.
- [44] T. Wang, C. Zhou, W. Xu, Online droplet monitoring in inkjet 3d printing using catadioptric stereo system, IISE Trans. 51 (2) (2019) 153–167.
- [45] T. Wang, T.-H. Kwok, C. Zhou, S. Vader, In-situ droplet inspection and closed-loop control system using machine learning for liquid metal jet printing, J. Manuf. Syst. 47 (2018) 83–92.
- [46] S.A. Razvi, S.C. Feng, A.N. Narayanan, Y.-T.T. Lee, P.W. Witherell, A review of machine learning applications in additive manufacturing, International Design Engineering Technical Conferences & Computers and Information in Engineering Conference (2019).
- [47] C. Gobert, E.W. Reutzel, J. Petrich, A.R. Nassar, S. Phoha, Application of supervised machine learning for defect detection during metallic powder bed fusion additive manufacturing using high resolution imaging, Addit. Manuf. 21 (2018) 517–528.
- [48] I.A. Okaro, S. Jayasinghe, C. Sutcliffe, K. Black, P. Paoletti, P.L. Green, Automatic fault detection for laser powder-bed fusion using semi-supervised machine learning, Addit. Manuf. 27 (2019) 42–53.
- [49] L. Scime, J. Beuth, Anomaly detection and classification in a laser powder bed additive manufacturing process using a trained computer vision algorithm, Addit.

- Manuf. 19 (2018) 114-126.
- [50] M. Khanzadeh, S. Chowdhury, M.A. Tschopp, H.R. Doude, M. Marufuzzaman, L. Bian, In-situ monitoring of melt pool images for porosity prediction in directed energy deposition processes, IISE Trans. 51 (5) (2019) 437–455.
- [51] M. Grasso, F. Gallina, B.M. Colosimo, Data fusion methods for statistical process monitoring and quality characterization in metal additive manufacturing, Proc. CIRP 75 (2018) 103–107.
- [52] A. Stetco, F. Dinmohammadi, X. Zhao, V. Robu, D. Flynn, M. Barnes, J. Keane, G. Nenadic, Machine learning methods for wind turbine condition monitoring: a review, Renew. Energy 133 (2019) 620–635.
- [53] S.J. Qin, Survey on data-driven industrial process monitoring and diagnosis, Annu. Rev. Control 36 (2) (2012) 220–234.
- [54] R. Zhao, R. Yan, Z. Chen, K. Mao, P. Wang, R.X. Gao, Deep learning and its applications to machine health monitoring, Mech. Syst. Signal Process. 115 (2019) 213–237
- [55] F. Sarrazin, K. Loubiere, L. Prat, C. Gourdon, T. Bonometti, J. Magnaudet, Experimental and numerical study of droplets hydrodynamics in microchannels, AIChE J. 52 (12) (2006) 4061–4070.
- [56] J. Shinjo, A. Umemura, Simulation of liquid jet primary breakup: dynamics of ligament and droplet formation, Int. J. Multiph. Flow 36 (7) (2010) 513–532.
- [57] E. Kim, J. Baek, Numerical study on the effects of non-dimensional parameters on drop-on-demand droplet formation dynamics and printability range in the up-scaled model, Phys. Fluids 24 (8) (2012) 82103.
- [58] M. Groot Wassink, Inkjet Printhead Performance Enhancement by Feedforward

- Input Design Based on Two-Port Modeling, Ph.D. Thesis, Delft University of Technology, Delft, 2007.
- [59] A.J. Chorin, Numerical solution of the Navier–Stokes equations, Math. Comput. 22 (104) (1968) 745–762.
- [60] T.J. Santner, B.J. Williams, W. Notz, B.J. Williams, The Design and Analysis of Computer Experiments 1 Springer, 2003.
- [61] T. Wang, T.-H. Kwok, C. Zhou, In-situ droplet inspection and control system for liquid metal jet 3d printing process, Proc. Manuf. 10 (2017) 968–981.
- [62] N. Srivastava, E. Mansimov, R. Salakhudinov, Unsupervised learning of video representations using lstms, International Conference on Machine Learning (2015) 843–852.
- [63] C. Finn, I. Goodfellow, S. Levine, Unsupervised learning for physical interaction through video prediction, Advances in Neural Information Processing Systems, (2016), pp. 64–72.
- [64] S. Xingjian, Z. Chen, H. Wang, D.-Y. Yeung, W.-K. Wong, W.-c. Woo, Convolutional lstm network: a machine learning approach for precipitation nowcasting, Advances in Neural Information Processing Systems, (2015), pp. 802–810.
- [65] D.P. Kingma, J. Ba, Adam: A Method for Stochastic Optimization, (2014) (arXiv preprint), arXiv:1412.6980.
- [66] Z. Wang, A.C. Bovik, H.R. Sheikh, E.P. Simoncelli, et al., Image quality assessment: from error visibility to structural similarity, IEEE Trans. Image Process. 13 (4) (2004) 600–612.
- [67] A.M. Saxe, P.W. Koh, Z. Chen, M. Bhand, B. Suresh, A.Y. Ng, On random weights and unsupervised feature learning, ICML, Vol. 2 (2011) 6.